

Indentation mechanics of Cu–Be quantified by an in situ transmission electron microscopy mechanical probe

M.S. Bobji^{a)}

Department of Mechanical Engineering, Indian Institute of Science, Bangalore, 560 012 India

J.B. Pethica

Department of Materials, University of Oxford, Oxford, OX1 3PH United Kingdom; and Physics Department, Trinity College, Dublin 2, Ireland

B.J. Inkson

Department of Engineering Materials, The University of Sheffield, Sheffield, S1 3JD United Kingdom

(Received 18 May 2005; accepted 28 June 2005)

In situ transmission electron microscopy was used to study, in real time, the sub-surface deformation taking place in Cu–Be alloy during nanoindentation. A twinned region of the material was indented with a sharp tungsten tip in a specially developed transmission electron microscopy (TEM) holder. A flexible hinge-based force sensor was used to measure the force on the indenter, and the force–displacement curve for the tip was obtained by tracking the tip in the sequential images of a TEM video of the indentation process. Step-like structures ~50 nm in size resulting from the tip surface roughness were observed to generate clusters of dislocations in the sample when they come in contact with the softer Cu–Be. With this setup, the forces and the mean pressure associated with such an individual deformation event in a nanostructured TEM sample were measured.

I. INTRODUCTION

Transmission electron microscopy (TEM) has been extensively used by materials scientists to study the deformation behavior of materials. The high resolution of TEM and the ability to look through the material have been used to decipher the deformation mechanisms of a wide variety of materials. Most of the TEM observations are post-mortem in the sense that the microstructural changes of the deformation frozen in the materials are analyzed in the TEM long after the application of the deforming forces and displacements and perhaps after creep and or aging. The postmortem approach does not, therefore, address the kinetics and the dynamics of the deformation as they happen during the deformation process. Few in situ experiments have been designed to overcome this handicap. There are two main ways in which the deformation can be induced in situ, either by using straining or by heating/cooling stages.

In TEM straining stages, the deformation is induced by mechanical means by pulling at a TEM sample, and in heating/cooling stages, the deformation is induced by temperature variations. In these experiments the local strains causing the deformation can be directly observed, though it is not possible to get an idea of the local

stresses. It is also difficult, especially at high magnifications, to observe a particular area of interest over an extended range of deformation, because with increasing deformation there is an increase in the global displacement, which causes the region of interest to shift. This difficulty can be overcome if the sample itself is made very small in length and the strains are applied locally.¹ Another way to address this difficulty is to use a mechanical probe to induce local deformation.

In the last few years, some in situ TEM holders have been built with mechanical probes employing differing means of actuation and sensing. Kizuka et al.² developed an in situ TEM tunneling probe to observe interactions between two gold tips at atomic resolution. Erts et al.³ developed an in situ atomic force microscope (AFM) that could observe jump to contact and measure adhesion between gold and the AFM tip. Wall et al.⁴ developed an in situ nanoindenter that used a piezoceramic actuator to indent using an attached diamond indenter, with Minor et al.⁵ measuring the force on the indenter by observing the difference in the piezoelectric translator's displacements under no load and loaded conditions. They were able to observe the pop-in event associated with the onset of the plastic deformation.

We built an in situ TEM mechanical probe holder, designed specifically for nanoindentation, with a compact mechanism to generate local deformation with a sharp tip and to measure force with a flexible hinges

^{a)}Address all correspondence to this author.

e-mail: bobji@mecheng.iisc.ernet.in

DOI: 10.1557/JMR.2005.0332

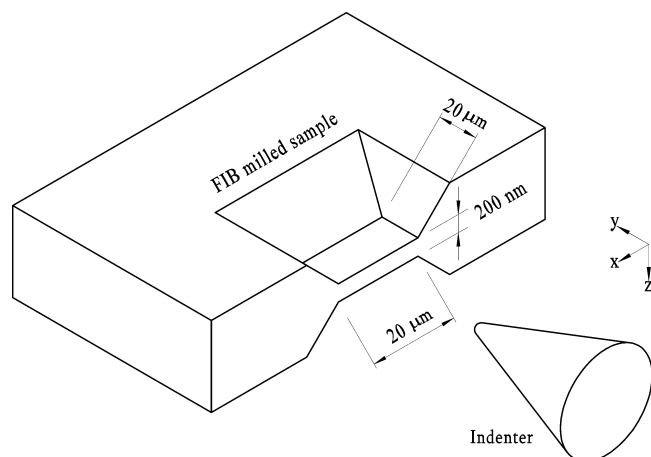


FIG. 1. Schematic illustration of the sample and the indenter showing the sample dimensions (not to scale).

based force sensor. To suit the material system being studied, the force sensor may be designed to operate at the required level of stiffness. Here we report the indentation mechanics of a Cu–Be alloy sample studied with the holder, clearly bringing out the capabilities of the holder.

II. EXPERIMENTAL

The in situ TEM holder^{6–8} was built to fit the JEOL 2010 and JEOL 3000F (Japan) series microscopes. The holder has the external geometry of the standard holders on the outside while on the inside it is hollowed out to fit the mechanisms that generate coarse and fine displacements. A 3-axis coarse positioner^{6,7} based on inertial sliders is used to get a sharp tip close to the sample within the range of the fine positioner. Miniaturization of this coarse positioner enabled us to achieve a compact design (about 10-mm in diameter and 100-mm in length) that can be accommodated within the vacuum chamber of the TEM. This minimizes the problems that arise due to mechanical vibration from the external environment and thermal drift.

The fine positioner of the nanoindenter⁸ consists of a four quadrant piezoelectric tube (PZT; diameter 6 mm).

The localized deformation in the sample is induced by pushing the tip into the sample with the help of this fine positioner. The resulting force is measured as the deflection of a spring element in a force sensor. The force sensor is a four-bar mechanism with conventional hinges replaced with flexible hinges designed to move linearly in a single two-dimensional (2D) plane. The force sensor has to be thin such that it can be accommodated within the pole piece of the microscope. The stiffness of the sensor, made by photo etching, can be varied by changing the web thickness of the hinges. The tip, made by electro-polishing tungsten wires 0.1 mm in diameter, is attached to the moving end of the force sensor.

The electron-transparent sample studied here was obtained from a Cu–Be foil (1.8% Be by weight) of 0.1 mm thickness. A focused ion beam microscope (FIB) was used to machine an electron transparent region of about 250 nm thick, 20 μm wide, and 5 μm deep (Fig. 1). The material surrounding the transparent region is given a gradual slope such that it can be easily located in the TEM. The electron transparent plane of the sample and the axis of the tip movement are aligned with the help of fresnel fringes at microscope magnifications greater than 100,000×.

The tip is moved at a constant velocity (~ 7.5 nm/s) toward the sample by applying a ramping voltage to all the quadrants of the piezoelectric tube. At maximum displacement, the voltage is held constant for 30 s before retracting with the same speed. The deformation events taking place during these periods were recorded continuously at 25 frames per second.

III. RESULTS AND DISCUSSION

Figure 2 shows a tungsten tip with a tip radius of about 100 nm indenting a twinned region of the Cu–Be sample. The three bright-field images show the tip and sample (a) coming just into contact, (b) at maximum displacement while holding, and (c) just moving out of contact.

The deformation zone includes a region of dark contrast to the left of the tip, visible in Figs. 2(b) and 2(c), interpreted as a cluster of dislocations (see Sec. III. A).

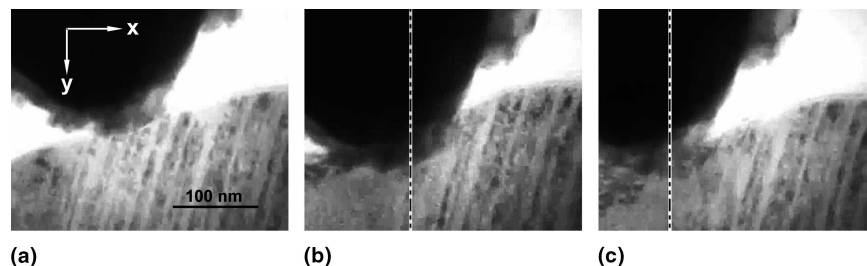


FIG. 2. Bright-field images showing the tip and sample: (a) coming just into contact, (b) at maximum displacement while holding, and (c) just moving out of contact respectively. The dashed lines are the axes along which the indenter is moving while loading in (b) and after breaking contact in (c). Between (b) and (c), the indenter has moved along the x -axis as well.

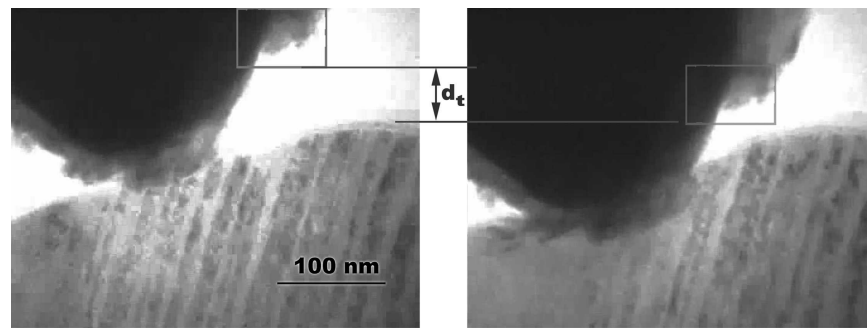


FIG. 3. Bright-field images showing the window chosen to measure the displacement of the indenter (d_t) by cross correlation through the various images.

The tip continues to move in a straight line (almost vertical in Fig. 2) in the image plane as it encounters the sample, but it has been observed to move at a steep angle to the left while unloading. By comparing Figs. 2(a) and 2(c), it can be clearly seen that the tip has moved to the left. This kind of asymmetric behavior with a net displacement of the tip perpendicular to the indentation axis has been observed in other samples as well.

The movement of the tip with respect to the sample is obtained from the series of still images obtained by digitizing the video frames. This is done by identifying a small portion of the tip containing some distinguishing features. The movement of that portion in subsequent images of the video is traced (Fig. 3) by cross-correlation. This gives the X and Y coordinates of the tip in the projection plane at any point of time with an accuracy of about one pixel. At 30,000 \times microscope magnification, this means that the minimum displacement of the tip that can be measured is 0.54 nm with our camera system.

Figure 4 shows the movement of the tip (d_t) in the X–Y plane, as obtained from the cross-correlations of the images during loading. The actual piezoelectric displacement (d_p) was obtained from the trajectory of the tip when it was moving in free space and not in contact with sample, for the same applied voltage. The difference between the two gives the deflection of the force sensor, i.e.,

$$d_f = d_p - d_t \quad .$$

If k is the stiffness of the force sensor then the force (F) can be obtained from⁶

$$F = kd_f \quad .$$

The stiffness of the force sensor was calibrated using a cantilever of a known stiffness and a heterodyne interferometer set up. The stiffness of the force sensor (k) used in this study is 1700 N/m.

A. Force–displacement curve

Figure 5 shows the load–displacement curve obtained while indenting a twinned region of copper–beryllium

alloy with a tungsten indenter. Depending upon the nature of the resistance offered by the sample to the penetration of the indenter, the loading curve can be divided into three distinct stages. In the first stage (I), the indenter–sample interaction is dominated by the asperities of the indenter and the sample. We take the contact point to be the point when the first visible asperities of the indenter and the sample touch. When the closest asperities are separated by about 3 nm, we see a small attractive force of about 0.5 μ N, barely resolved over the background noise. As the indenter displacement increases, contact is established at other asperities [Fig. 6(a)], and the load increases (stage I in Fig. 5). When the penetration of the indenter into the sample is about 10 nm from the initial contact point, we can no longer distinguish the individual asperities.

The second stage (II) of the Cu–Be indentation is marked distinctively by the straight line portion of the load–displacement curve. At this stage, the indenter tip can be approximated [Fig. 6(b)] to a sphere of radius 100 nm with some roughness imposed on it. If the elastic half space assumption holds good, as the contact radius

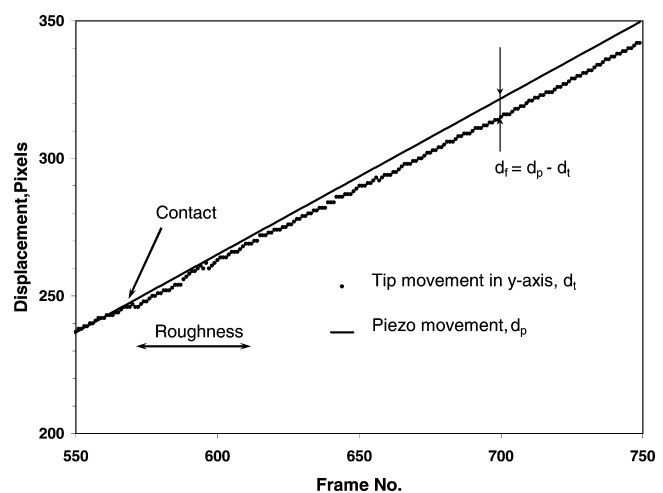


FIG. 4. Displacement (d_t) of the indenter along the vertical axis from the different frames of the video. The straight line is the displacement (d_p) generated by the piezoelectric positioner. The force sensor deflection is given by $d_f = d_p - d_t$.

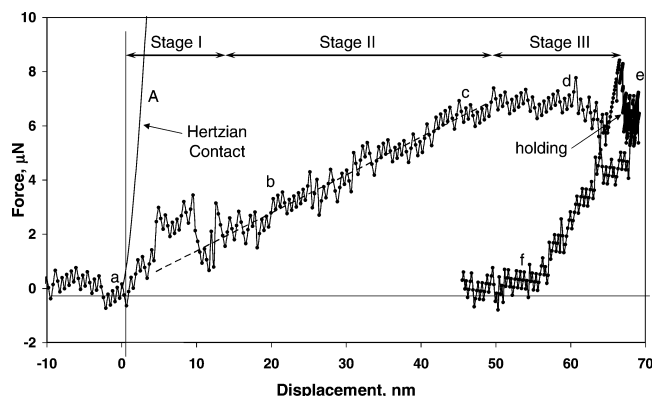


FIG. 5. Force–displacement curve for the first indentation on the Cu–Be sample. In stage I, the sample and the indenter roughness dictate the behavior and in stage III, a dislocation cluster is formed due to the surface step I on the indenter. The TEM bright field images at the different points (a–f) along the curve are given in Fig. 6.

(about 30 nm) is small compared to the width of the FIB sample (about 250 nm), the Hertzian analysis⁹ for this contact is as plotted as curve A in Fig. 5. It can be clearly seen that the measured load is much smaller than that expected in an elastic contact on a bulk sample. The likely cause is that the FIB sample has a rounded edge; i.e., there is a reduction in thickness close to the edge of the sample. This can result from the FIB milling process when incident ions sputter away the material from the specimen edge as well as the sides. The thickness of the amorphous layer on the sample is few nanometers as observed at higher magnifications.

For a spherical indenter of radius R , the load P on the indenter, for a given penetration depth h , is given by

$$P = p_m \pi a^2 = \pi P_m (2 R h - h^2) \approx 2 \pi R p_m h ,$$

where a is the contact radius and p_m is the mean pressure. For fully plastic indentation, the mean pressure is constant and is approximately 3 times the yield stress.⁹ Thus in stage II, as the load is directly proportional to the penetration, the material appears to be fully plastic. In this stage [Fig. 6(c)], we see some of the alternating contrast from the twinned regions disappear, but no dislocation activity is observed in the current diffraction condition. The mean pressure in this stage, estimated from Fig. 5, is about 180 MPa.

The stage II regime exists until a penetration depth of about 40 nm; thereafter, in stage III, the load remains more or less constant as the penetration increases, followed by a sharp increase in load. Looking at the TEM images, this stage is dominated by the generation and propagation of a dislocation cluster on the left hand side of the indenter. The edge of the indenter is rough, and it can be seen from Fig. 6(c) that there is a step-like structure on the indenter surface. This means that the contact width does not increase with the penetration, as can be seen from Fig. 6(d). This introduces a high stress concentration, which in turn is responsible for the sudden spurt of dislocation generation. As the penetration increases, the dislocation cluster increases in size but is localized close to the step and the specimen surface. The dislocations are observable at maximum radial distance of 45 nm from the step. The indenter step rapidly becomes surrounded by the deformed material [Fig. 6(e)], and the load increases suddenly.

After stage III, while the indenter is held with a constant piezoelectric voltage, the load decreases slightly

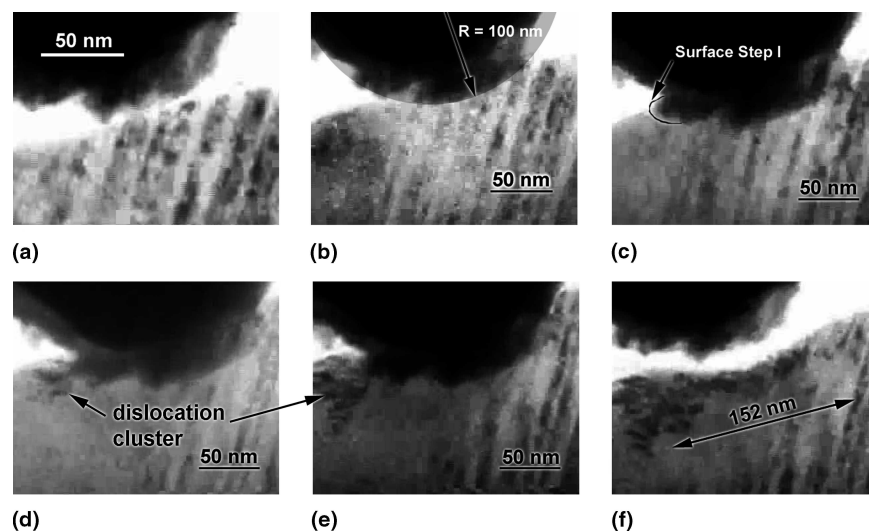


FIG. 6. Digitally magnified video frames from the TEM during the indentation process. Time t elapsed since the start of the indentation process is given in the brackets for each image. (a) Interaction of the roughness ($t = 18.12$ s). (b) The indenter tip can be approximated to a sphere of 100 nm radius in stage II ($t = 20.64$ s). (c) Some of the contrast from the twinned region changes. The surface step I of the indenter comes into contact ($t = 23.72$ s). (d) The dislocation cluster being generated by the stress concentration resulting from the surface step ($t = 26.52$ s). (e) At the maximum penetration of the first indentation after the hold ($t = 58.92$ s). (f) The residual impression after the first indent ($t = 66.56$ s).

with no visible change in the sample contrast. When the indenter is retracted, it is observed that the indenter starts moving left toward the dislocation zone. As soon as the contact is broken (the load becoming zero), the indenter starts moving along the direction parallel to the loading direction. From the residual impression left by the indenter in Fig. 6(f), it can be seen that there are no visible pile-up effects for this indentation. The region over which there has been some visible transformation can be approximated to a hemispherical envelope of about 110 nm. Assuming that this could be the elastic plastic boundary, the elastic-plastic boundary to contact radius ratio (ca) is about 1.5. The spherical cavity model⁸ gives 2.3 for this condition.

B. Reloading

Figure 7 shows the load–displacement behavior when the Cu–Be sample is indented a second time at the same sample position as the previous indent. In the second cycle, there is a marked increase in the adhesion force as the asperities interact. The asperity of the indenter that comes into contact first on reloading has a larger radius of curvature than that which came into contact first in the previous cycle. As the contact develops further, initially the indenter matches the profile of the residual impression left. At this stage, the load displacement curve matches with that of the previous cycle. The load increases suddenly when the step I [Figs. 6(c) and 8] on the indenter surface comes into contact, and as before, the load then remains constant with the dislocation tangle close to the step increasing in size with increasing displacement. The step contacts the sample slightly to the left of the site where it touched the sample before. A visible band of dislocations develops around the indenter as the penetration increases. There are further sudden increases in the load as the other features of the indenter

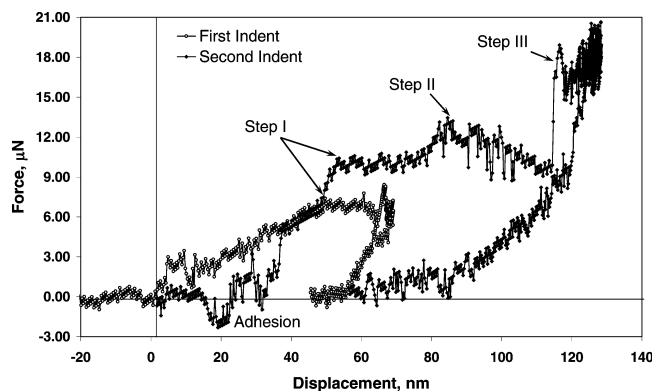


FIG. 7. Force–displacement curve resulting from indenting the residual impression left from the first indent. The second indentation exhibits higher adhesion (negative force in the graph). The curve deviates from the first curve as the step I comes into contact at slightly a different position. As the indenter surface steps II and III come into contact, they leave their signature on the curve.

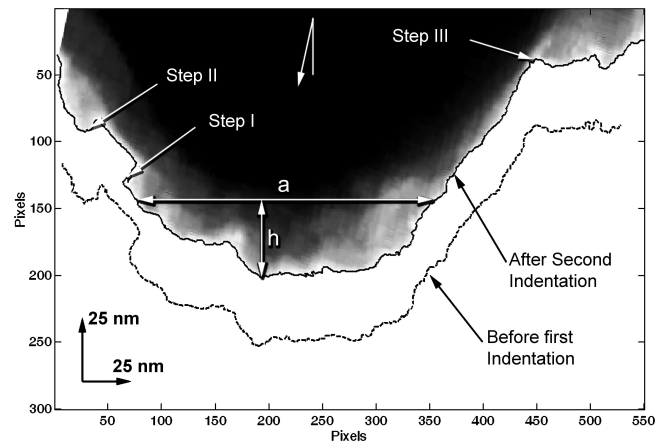


FIG. 8. Edge profiles of the indenter obtained from the TEM images. There is very little (less than 5 pixels = 2.7 nm) difference between the profiles before indentation and after two indentations. The image has been rotated such that the vertical axis coincides with the normal to the mean sample surface. The roughness has been enhanced for visualization by having a higher vertical magnification. The arrow at the top indicates the direction of indenter movement during the loading part of the indentation.

come into contact with the sample (steps II and III in Figs. 7 and 8).

C. Analysis of indenter and sample profiles

The edges of the sample and the indenter could be identified in the bright-field TEM images from the sharp jump in the electron intensity value between the material and the background. The edge profiles of indenter and the sample are presented in Figs. 8 and 9 respectively. It should be noted that, for visualization purposes, the vertical and horizontal scales in these figures are not the same and thus roughness appears to be accentuated. Very low contrast in this particular diffraction condition at

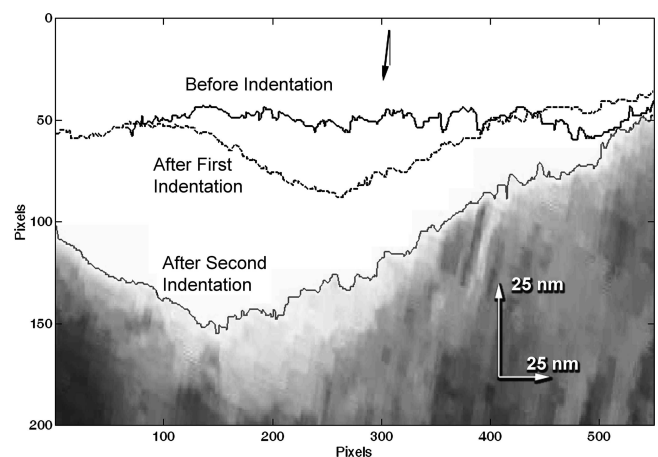


FIG. 9. Edge profiles of the sample showing the size and the shape of the residual impressions. The roughness has been enhanced by higher vertical magnification. The arrow indicates the direction of indenter motion.

some of the twinned regions is also responsible for showing higher apparent roughness of the undeformed sample.

The indenter, being made of the high atomic number tungsten, is almost completely opaque to 200 kV electrons except for the regions close to the apex (see, for example, Fig. 2). It was almost impossible to obtain a diffraction pattern from the tip. This is probably due to a mixture of inelastic electron scattering and the presence of some contamination/oxidation from the electropolishing preparation route. The thin regions of the indenter tip survived the high indentation pressure, and there is very little change in the morphology with penetration as can be seen from Fig. 8, indicating that at least a part of the transparent region is not just mechanically soft carbon contamination.

Comparing the edge profiles and contrast of the indenter before and after the indentation suggests that there is very little transfer of the material from the sample to the tip. It is quite possible that there is some actual material transfer, but we are not able to resolve it within the current experimental conditions. The increased attractive force during the approach for the second indent (Fig. 7) could be due to the contact occurring between similar materials.

The mean line of the sample profile obtained is inclined to the axis of the indenter motion by 75° (Fig. 9). This means that the indentation was carried out on the surface that is locally inclined. The root-mean-square (rms) roughness of the sample edge profile is about 2.39 nm measured over a length of 300 nm. This roughness will be different from those obtained by stylus type measurements as this measurement is done on the projected profile of a sample up to 250 nm thick. Some of the imaged asperities of the indenter and the sample do not touch as they are in different Z-planes.

From the sample profiles, the projected area of the residual impression can be estimated by assuming that the indenter is axisymmetric. The measured contact diameter is about 160 nm for residual impression after first indent and 310 nm for the second indent. This gives estimated “hardness” values for the nanostructured Cu–Be TEM samples as 390 and 270 MPa, respectively. The hardness for the same material measured with a nanoindenter (Hysitron Inc.) varied between 2 and 4.2 GPa. This nanohardness was obtained by indenting the Cu–Be sample away from the FIB thinned area with a diamond berkovich indenter with the maximum penetration ranging from 50 to 80 nm.

D. Contact pressure variation

The area function of the indenter is a function that gives the cross-sectional area of the indent for different penetration depths. In depth-sensing indentations, the area function is used to obtain the hardness of the material from the measured load and penetration.^{10–12} Any

error in the determination of the area function leads to appreciable error in the hardness values for very small penetration depths¹³ (<100 nm). The area function is typically obtained by indenting soft materials and observing the indent in electron microscopes at high resolution.

From the indenter profile (Fig. 8), we can obtain the width a of the indenter for different penetration depths (h). We assume that the indenter is axisymmetric and obtain the area function of the indenter. Figure 10 shows the variation of the indenter width and the actual contact width measured from the bright-field images for the first indent. The close match for the small penetration means that there is negligible pileup or sink-in. The figure also shows the contact width for the best fit spherical tip. In depth-sensing experiments, the sample and the indenter are assumed to be smooth, and the area function is obtained from the first contact point. The error introduced due to the roughness can be accounted for by introducing a correction factor (h_c) to the measured penetration depth (h).^{13,14} The correction factor for the first indent is about 4 nm which is comparable to the sample rms roughness of 2.39.

From the measured area function, the contact pressure variation with penetration is obtained for the first indent and is plotted in Fig. 11. Up to a depth of about 20 nm, the scatter in hardness variation is high. It seems that the increased mean pressure and the scatter in hardness occur in the region where the surface roughness could be playing an important role. The mean pressure drops to about 280 MPa in stage II. At this stage, the indenter contact width (100–150 nm) is at least half the maximum sample width (~250 nm) and hence the plastic deformation zone would have reached the surfaces (see Fig. 11, inset). This

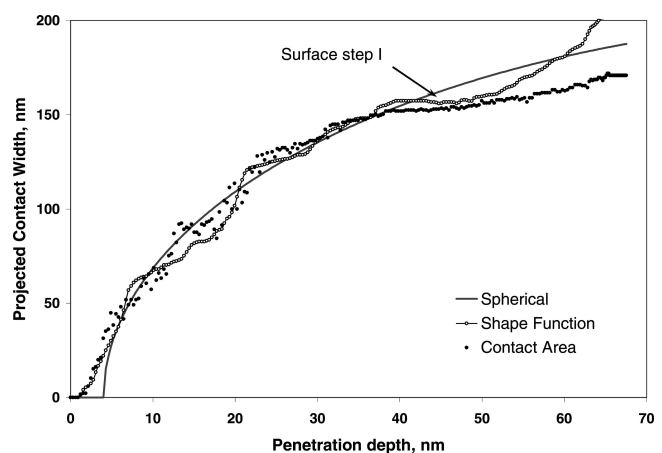


FIG. 10. Variation of projected contact width with indenter penetration. The width measured from the TEM images (black dots) matches closely with the width (a) of the indenter obtained from Fig. 9 for different penetration depths (h). The contact width obtained from the spherical tip approximation is plotted as the continuous line for comparison.

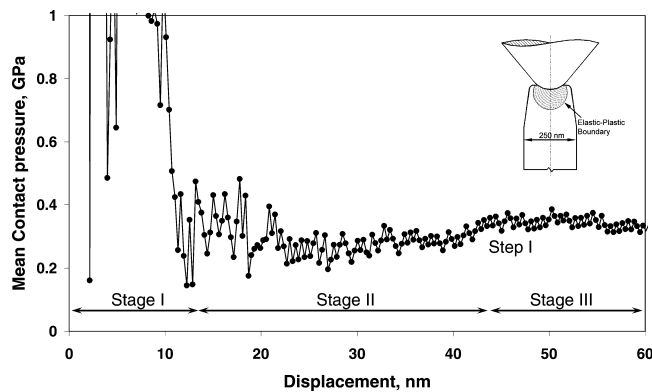


FIG. 11. Variation of the calculated mean contact pressure with the indenter displacement. There is slight increase in the mean pressure as step I comes into contact with the sample. The inset shows a schematic illustration of the sample and the indenter geometry.

means that the measured mean pressure will be less than the hardness of the material due to the loss of constraint exerted by the surrounding elastic zone. For example, for a fully plastic condition, the mean pressure to yield stress ratio is about 3, as given by the spherical cavity model, while the ratio reduces to about 2 for plane stress indentation with a 120° wedge angle. In stage III, in which the surface step induces a dislocation cluster, the pressure increases to 350 MPa.

The absence of any appreciable indentation size effect could be due to the fact that the region selected for indentation could be high in defect concentration to start with, i.e., many twin boundaries and probable associated dislocations. The low elastic modulus to yield stress ratio for the Cu–Be alloy means that for a penetration of 10 nm the material is already in the fully plastic region.⁸ The effect of loss of constraint, at higher penetration depths for the TEM-compatible specimen geometry used, could also be one of the reasons why the size dependency is not observed.

IV. CONCLUSIONS

We have demonstrated that in situ TEM nanoindentation is a powerful technique for studying the deformation mechanics of the materials at the nanoscale. The forces and the mean pressure associated with an individual deformation event in a nanostructured TEM sample, such as the generation of dislocation cluster resulting from the stress concentration caused by a surface step on the indenter, have been measured and directly associated with real-time imaging of the dynamical event. Though it is

not meaningful to talk about the “hardness” in its traditional sense in these investigations, since the elastic constraint to the normally confined plastic zone is lost due to the thin TEM-compatible sample geometry, it is found that the measured mean pressure values during deformation for the twinned region of the thin sample of Cu–Be alloy are much smaller than the values obtained from nanoindentation.

REFERENCES

1. M.A. Haque and M.T.A. Saif: In situ tensile testing of nano-scale specimens in SEM and TEM. *Exp. Mech.* **42**, 123 (2002).
2. T. Kizuka, K. Yamada, S. Deguchi, M. Naruse, and N. Tanaka: Cross-sectional time-resolved high-resolution transmission electron microscopy of atomic-scale contact and noncontact-type scannings on gold surfaces. *Phys. Rev. B* **55**, R7398 (1997).
3. A. Erts: Löhmus, R.Löhmus, H. Olin, A.V. Pokropivny, L. Ryen, and K. Svensson: Force interactions and adhesion of gold contacts using a combined atomic force microscope and transmission electron microscope. *Appl. Surf. Sci.* **188**, 460 (2002).
4. M.A. Wall and U. Dahmen: An in situ nanoindentation specimen holder for a high voltage transmission electron microscope. *Microsc. Res. Technol.* **42**, 248 (1998).
5. A.M. Minor, J.W. Morris, Jr., and E.A. Stach: Quantitative in situ nanoindentation in an electron microscope. *Appl. Phys. Lett.* **79**, 1625 (2001).
6. M.S. Bobji, C.S. Ramanujan, R.C. Doole, J.B. Pethica, and B.J. Inkson: An in situ TEM nanoindenter system with 3-axis inertial positioner, in *Mechanical Properties Derived from Nanostructuring Materials*, edited by D.F. Bahr, H. Kung, N.R. Moody, and K.J. Wahl (Mater. Res. Soc. Symp. Proc. **778**, Warrendale, PA, 2003), p. 105.
7. M.S. Bobji, C.S. Ramanujan, J.B. Pethica, and B.J. Inkson: *Proceedings of International Congress on Electron Microscopy, Durban*, 941 (2002).
8. M.S. Bobji, C.S. Ramanujan, J.B. Pethica, and B.J. Inkson: A miniaturized TEM nanoindenter for studying material deformation in situ. *Meas. Sci. Technol.*, (submitted).
9. K.L. Johnson: *Contact Mechanics* (Cambridge University Press, Cambridge, U.K., 1985).
10. W.C. Oliver and G.M. Pharr: An improved technique for determining hardness and elastic modulus using load and displacement sensing indentation experiments. *J. Mater. Res.* **7**, 1564 (1992).
11. M.F. Doerner and W.D. Nix: A method for interpreting the data from depth-sensing indentation instruments. *J. Mater. Res.* **1**, 610 (1986).
12. K. Herrmann, N.M. Jennett, W. Wegener, J. Meneve, K. Hasche, and R. Seemann: Progress in determination of the area function of indenters used for nanoindentation. *Thin Solid Films* **377–378**, 394 (2000).
13. M.S. Bobji and S.K. Biswas: Deconvolution of hardness from data obtained from nanoindentation of rough surfaces. *J. Mater. Res.* **14**, 2259 (1999).
14. H-J. Weiss: On deriving Vickers hardness from penetration depth. *Phys. Status Solidi A* **99**, 491 (1987).